ELSEVIER

Journal of Nuclear Materials 257 (1998) 134–144

journal of nuclear materials

# Investigation of liquid impact erosion for 12Cr steel and Stellite 6B

Min Ku Lee [a], Whung Whoe Kim [b], Chang Kyu Rhee [b], Won Jong Lee [a,*]

[a] *Department of Materials Science and Engineering, Korea Advanced Institute of Science and Technology, 373-1 Kusong-dong, Yusong-gu, Taejon, 305-701, South Korea*

[b] *Advanced Nuclear Materials Department, Korea Atomic Energy Research Institute, Taejon, 305-353, South Korea*

Received 31 March 1997; accepted 18 May 1998

**Abstract**

A study has been made on the liquid impact erosion mechanisms of 12Cr steel and Stellite 6B (Co–28Cr) currently used as steam turbine blade materials. 12Cr steel underwent the transition from ductile to brittle deformation behavior during liquid impacts. Damage started with the formation of isolated hollows. The increase in density and the overlapping of these hollows resulted in surface undulations with repeated impacts. The cumulative liquid impacts produced a work hardened surface, followed by the material loss due to crack formation and propagation. The deformation in Stellite 6B was especially governed by its microstructure. The carbide precipitates were selectively eroded while the precipitate–matrix interface and the precipitate interior acted as initiating sites for cracks. The damage of the cobalt matrix, where the mechanical twins were formed, was much lower than that of the carbide precipitates. 

*PACS:* 92.40.G

## 1. Introduction

Erosion of steam turbine blades, especially the last low pressure ones, in nuclear power plants has been a significant problem throughout steam turbine history in terms of turbine performance, efficiency, safety, and lifetime. Erosion occurs by the collision of water drops in steam with high speed rotating blades. 12Cr steel and Stellite 6B have been used as a blade body material and as a shield material on blade leading edge which are subjected to the most significant erosion. However, both the blade body material and the shield material also eroded at a higher rate than desired as shown in Fig. 1. Many studies have been made on shielding with more erosion-resistant material [1–4] and the alloy design of blade materials [5] to solve the erosion problem. First of all, in order to improve the erosion resistance of blades, the erosion mechanisms of the conventional blade materials should be studied and precisely understood. Such a study, however, has not yet been sufficiently made. In the present study, the water impact erosion mechanisms of 12Cr steel and Stellite 6B used as blade component materials were investigated.

## 2. Experimental

The samples prepared for erosion testing were 12Cr steel and Stellite 6B used as a blade material and a shield material, respectively. Their compositions and physical and mechanical properties are given in Table 1. All samples were disc shaped with a thickness of 1.5 mm and a diameter of 15 or 25 mm. They were all mirror-polished by 1 μm $Al_2O_3$ powder.

The whirl arm type [6] and the disk rotary type [7,8] have been widely used as a standard erosion tester but have some disadvantages such as a limitation in speeds

* Corresponding author. Tel.: +82-42 869 4257; fax: +82-42 869 3310; e-mail: wjlee@cais.kaist.ac.kr.

0022-3115/98/$ – see front matter 
PII: S0022-3115(98)00440-1

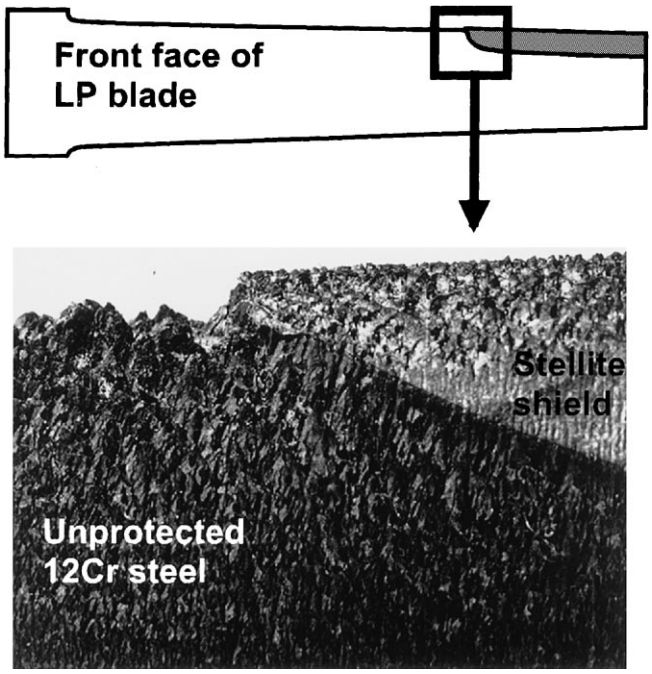


Fig. 1. Eroded surface of LP last rotating steam turbine blade.

Table 1
Physical and mechanical properties of blade materials

| | 12Cr steel | Stellite 6B |
|---|---|---|
| Composition (wt%) | 12Cr, 0.3Mn, 0.1C, bal. Fe | 28Cr, 4W, 3Ni, 2Si, 1.2C, bal. Co |
| Density (g/cm$^2$) | 7.70 | 8.38 |
| Poisson ratio ($v$) | 0.26 | 0.3 |
| Elastic modulus (GPa) | 217 | 209 |
| Yield strength (MPa) | 589 | 633 |
| Tensile strength (MPa) | 765 | 1110 |
| Vickers hardness (kg/mm$^2$) | 380 | 420 |

attainable, high power consumption, and vibrations due to unbalancing. Hence, an erosion tester was designed, which could attain speeds above 300 m/s and allow multiple impact. Its fundamental design has been submitted for a Korean patent [9] and is shown in Fig. 2. Once the desired pressure was achieved in the air reservoir (above 1.3 bar), this compressed air was passed down into the main cylinder. The nylon piston located initially at the upper position of the main cylinder was pushed down due to the compressed air. The nylon piston subsequently pushed the T-piston in the main cylinder. The water in the nozzle, supplied continuously by a peristaltic pump, was ejected by the T-piston. All operations were in sequence controlled by a computer. The water speed was measured by a velocimeter in the 10 mm gap between the nozzle orifice and the specimen. The diameter and length of the nozzle orifice were 0.5 and 3 mm, respectively and the nozzle-to-specimen

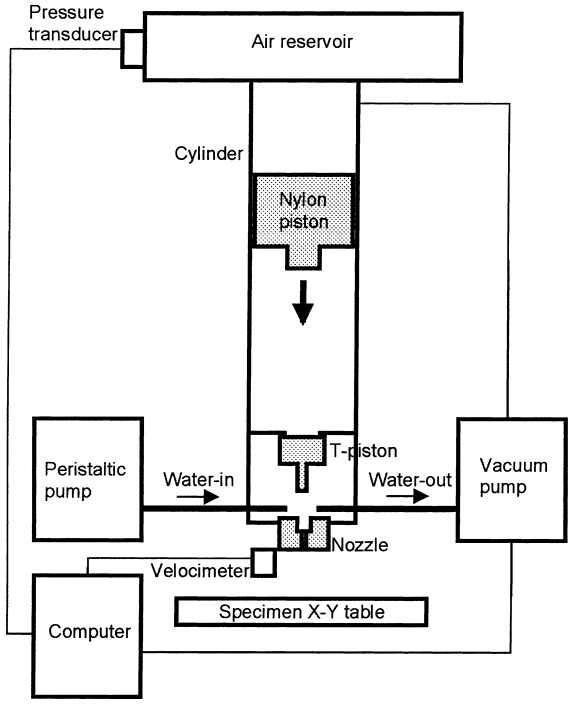


Fig. 2. Schematic diagram of liquid jet apparatus.

distance was 11 mm. The impact angle of the water was constantly 90° and the volume of the water per impact was about 0.15 $cm^3$. The erosion test was performed in air and at room temperature. The eroded surfaces of samples were observed by using an optical microscope and a scanning electron microscope.

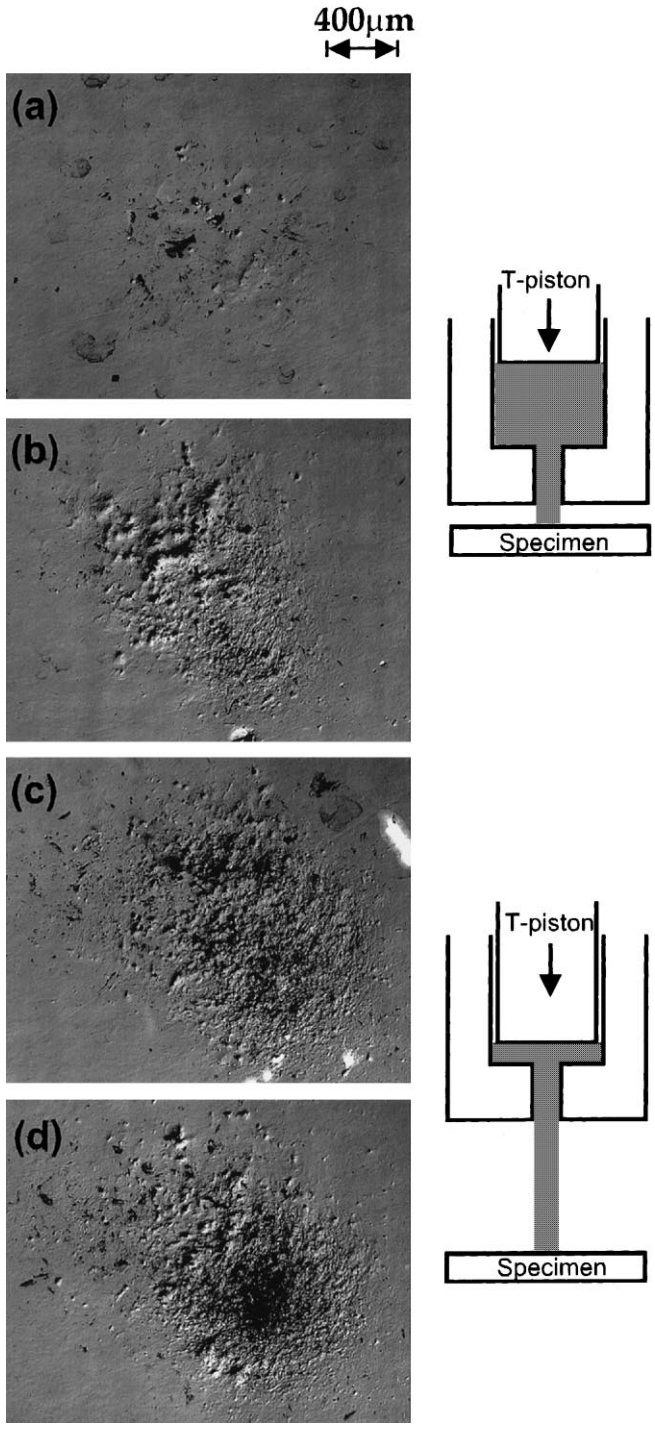


Fig. 3. Erosion damage of 12Cr steel with nozzle-to-specimen distance after 20 impacts at an impact velocity of 363 ± 20 m/s: (a) 2 mm, (b) 5 mm, (c) 8 mm and (d) 11 mm.

## 3. Results and discussion

### 3.1. Effects of nozzle-to-specimen distance

In order to obtain the severe erosion damage condition, the damage of the material was observed with respect to the nozzle-to-specimen distance which was a test parameter sensitive to erosion damage. Fig. 3 shows the erosion damage produced on 12Cr steel after 20 impacts at an impact velocity of 363 ± 20 m/s when the nozzle-to-specimen distance changed from 2 to 11 mm (the maximum distance was 11 mm in this design). The erosion damage became severe with increasing nozzle-to-specimen distance. The variation in degree of damage indicated that the impact velocity of water changed with the nozzle-to-specimen distance.

When the water comes out of the nozzle, its initial velocity may be determined by the moving velocity of the T-piston according to Bernoulli's theory. Once the water comes out, it is subject to air friction and gravitation. The gravitation is constant, whereas the frictional force in air is proportional to the transport velocity of a body as long as the motion is not too fast. If the frictional force in air is lower than the gravitation, the transport velocity of a body will increase (e.g. free falling) and if not, the transport velocity of a body will decrease. After a critical time at which the frictional force in air becomes equal to the gravitation, a body will be in uniform motion because the acceleration becomes zero. Therefore, as the nozzle-to-specimen distance decreases, the velocity of water will increase to more than the measured value of 363 ± 20 m/s at a distance of 10

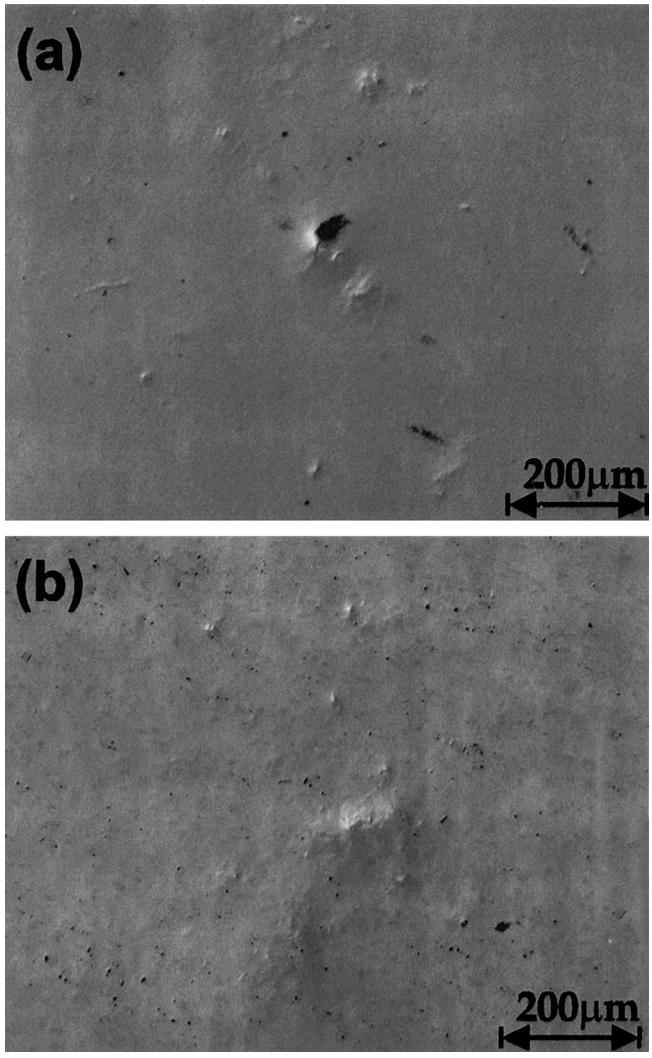


Fig. 4. Single impact damage on: (a) 12Cr steel at 323 m/s and (b) Stellite 6B at 342 m/s.

mm from the nozzle and the resultant damage will increase.

However, the test results showed that the damage became more severe as the nozzle-to-specimen distance increased. This phenomena could be explained in terms of the moving velocity of the T-piston. For small nozzle-to-specimen distance, the T-piston will experience early the back pressure of the water since the water is in contact with the specimen before the T-piston fully acts, which will result in a decrease in the moving velocity of the T-piston. The water coming out of the nozzle then strikes the specimen with a lower velocity. For larger nozzle-to-specimen distance, however, the T-piston will not experience the back pressure of the water since there is enough time for larger volume of water traveling to the specimen with high velocity. Finally, as the nozzle-to-specimen distance decreases, the initial velocity of the water in contact with the specimen increases. This is due to a decrease in the exposure time to air friction. But afterwards the velocity of the water decreases due to a decrease in the moving velocity of the T-piston. The damage of Fig. 3, therefore, suggests that the impact velocity of the water decreased greatly due to the decrease in the moving velocity of the T-piston rather than due to air friction. The increase over a certain nozzle-to-specimen distance would, however, be expected to result

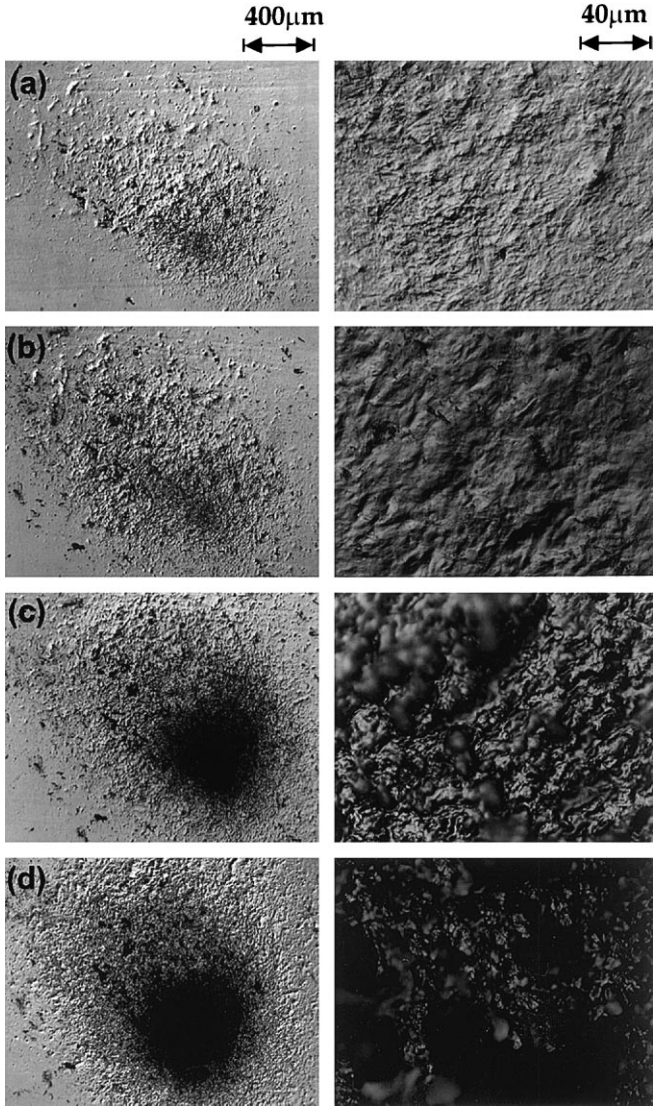


Fig. 5. Development of erosion damage in 12 Cr steel with increasing impact number at an impact velocity of 350 ± 20 m/s: (a) 30, (b) 90, (c) 130 and (d) 290.

in a weakening of damage because the decrease in the impact velocity of water due to air friction would become more dominant than the decrease in the moving velocity of the T-piston.

### 3.2. Single impact damage

Fig. 4 represents single impact damage produced on 12Cr steel and Stellite 6B. It was observed that several isolated hollows, i.e. deformation without cracks or local fracture, different in size were formed throughout a damage area of diameter 0.8 to 1 mm. Single impact damage showed that the liquid striking the specimen consisted not of a continuous liquid phase but of separated individual liquid phase droplets. The different diameters and depths of the hollows formed on the surface are related to the impingement droplet sizes and the impingement intensities, respectively.

### 3.3. Liquid impact erosion mechanisms of 12Cr steel and Stellite 6B

Fig. 5 shows the development of erosion damage in 12Cr steel with increasing number of impacts at an impact velocity of 350 ± 20 m/s. The very early damage observed in 12Cr steel consisted of several isolated hollows as shown in the single impact damage of Fig. 4(a). As the impact number increased, the density of the hollows increased and then the surface was continuously undulated by the overlapping of these hollows as shown in Fig. 5(a). The cumulative impacts intensified surface distortion (Fig. 5(b)) and the small craters, i.e. deformation with cracks or local fracture, were subsequently produced with preferential erosion at weakened sites (Fig. 5(c)), followed by the growth of the larger and deeper craters (Fig. 5(d)). 12Cr steel showed a ductile behavior below a certain impact number, featured by

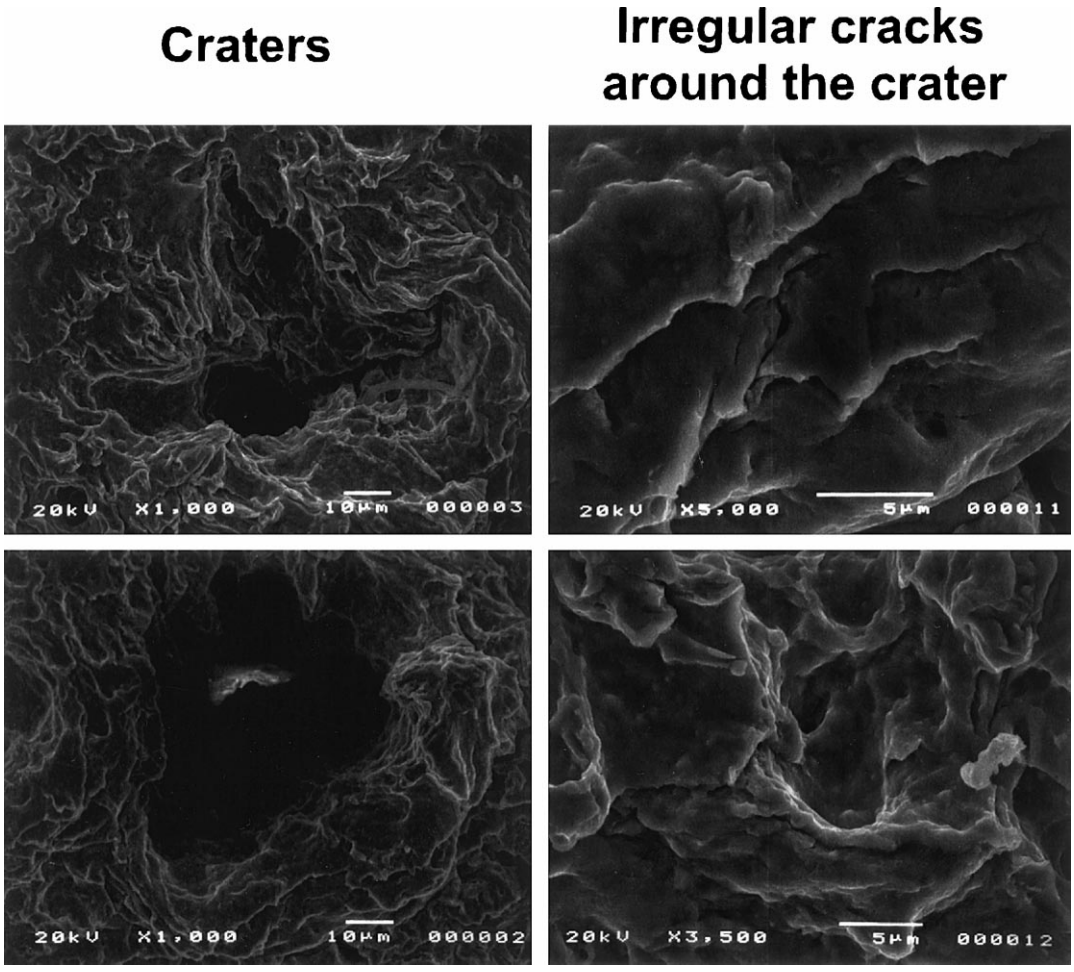


Fig. 6. Scanning electron micrographs showing the craters and the surrounding cracks produced on 12Cr steel after 290 impacts at an impact velocity of 350 ± 20 m/s.

continuous surface undulation, without loss of material (Fig. 5(a) and (b)). The behavior then changed into a brittle one in that cracks and local fracture were extended over the surface by liquid impact induced work hardening. The brittle deformation of 12Cr steel may be seen in Fig. 6 which shows the craters and the surrounding cracks formed irregularly after 290 impacts at an impact velocity of 350 ± 20 m/s, respectively. The deep craters had sizes in the range of 50 μm of depth and 60–70 μm of width to 4 μm of depth and 6 μm of width, indicating that the weakened sites were preferentially eroded. The irregular shape of the crater shown in Fig. 6 demonstrated the development of erosion damage by the crack propagation around the sites eroded initially.

Cobalt-base alloys (e.g. Stellite 6B) have been recognized as an alloy type most resistant to both cavitation erosion and liquid impact erosion [10]. The underlying reasons for their superior erosion-resistant behavior, however, are not yet clear. Investigations have attempted to obtain a correlation between the erosion of the materials and the mechanical properties such as hardness and strain energy to fracture but all such attempts have been unfortunately unsuccessful. For example, austenitic stainless steels had higher erosion resistance than martensitic stainless steel of the same hardness and cobalt-base alloys had much higher resistance in relation to hardness [11]. The strain energy to fracture of aged Haynes alloy No. 718 (Co-base alloy) was five times greater than that of Stellite 6B (Co-base alloy), but the cavitation erosion resistance of aged Haynes alloy No. 718 was actually two times less than that of Stellite 6B [12]. According to micro-Vickers hardness tests carried out in this study, 12Cr steel and Stellite 6B were about 380 and 420 kg/mm$^2$ respectively which were not too different (see Table 1). However, the liquid impact erosion resistance of Stellite 6B was at least six times greater than that of 12Cr steel, implying that hardness is not the governing factor for liquid impact erosion. Stellite 6B also showed very different behavior in liquid impact erosion in comparison with 12Cr steel. Stellite 6B generally had a 2-phase structure as shown in Fig. 7 in which coarse (5–20 μm) and hard carbides of $M_7C_3$ (M = Cr) and $M_6C$ (M = W, Mo) were dispersed in a matrix of ductile Co-rich solid solution. Fig. 8 shows how this microstructure changed sensitively with increasing number of impacts. The initial deformation of Stellite 6B appeared as surface undulations due to the formation and superposition of hollows as for 12Cr steel. The surface distortion intensified with increasing number of impacts (Fig. 8 (a)–(d)), but the maximum damage depth was no more than 3–4 μm in the cobalt matrix, not as severe as for 12Cr steel. A notable characteristic of the cobalt matrix was the formation of mechanical twins as observed in Fig. 8. The formation of twins in Co single crystals or Co alloys by mechanical working or cavitation shock has already been reported in

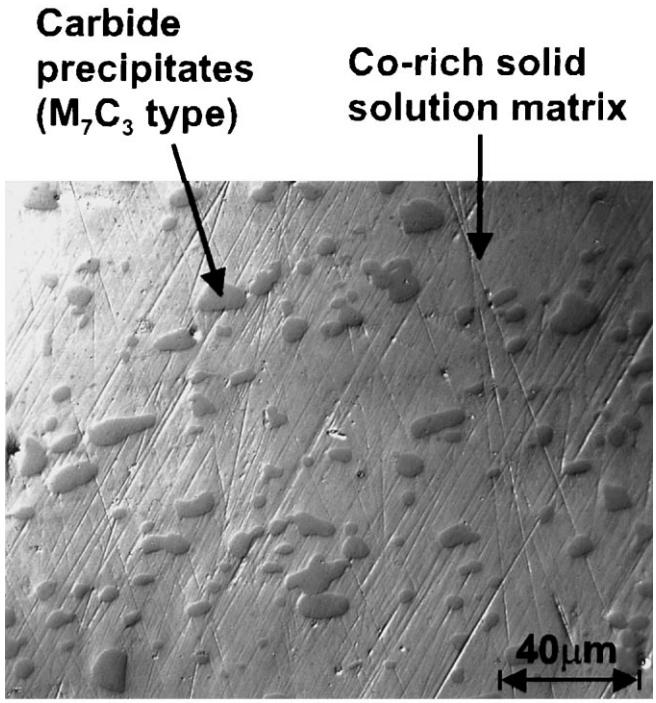


Fig. 7. Typical microstructure of Haynes Stellite alloy No. 6B.

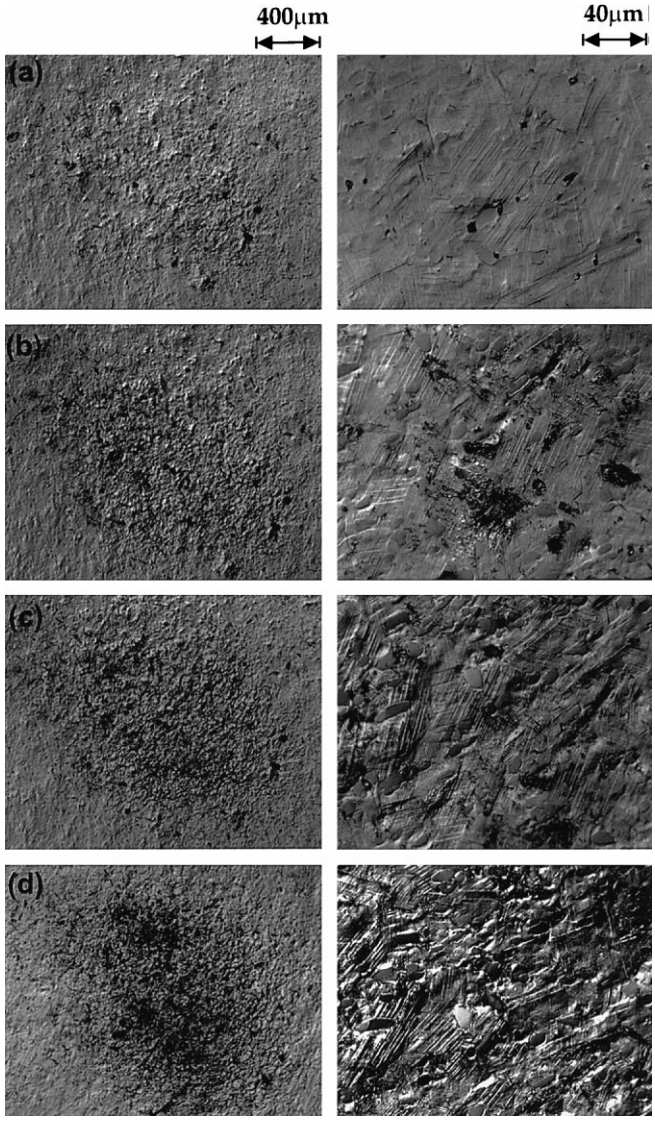


Fig. 8. Development of erosion damage in Stellite 6B with increasing impact number at an impact velocity of 350 ± 20 m/s: (a) 30, (b) 90, (c)130, (d) 290.

the literature [13–17]. As the impact number increased, the density of twins was found to increase and cracks were eventually formed at the twin boundaries as shown in Fig. 9. These cracks seemed to be fatigue cracks produced by the cumulative impact loadings. The resultant deformation of the cobalt matrix by liquid impacts appeared mostly as the twins accompanied with small surface undulations. There seemed to be little or no erosion of the cobalt matrix up to 290 impacts. Material loss in Stellite 6B was observed at the carbide precipitates. All the carbide precipitates were fractured after 290 impacts at an impact velocity of 35 ± 20 m/s and their damage was classified into three features as shown in Fig. 10; local fracture of the precipitate (A), propagation of the crack along the interface or the interior of precipitate (B), and removal of the precipitate (C). It followed from this that precipitate damage started with the formation and propagation of cracks along the interface or the interior (Fig. 11(a)), followed by the removal of the precipitate (Fig. 11(b)). After 290 impacts, the damage depth of precipitate was 5–10 μm deeper than in the matrix. Thus material removal from Stellite 6B was more dominant in the carbide precipitates than in the cobalt matrix. The erosion behavior of Stellite 6B by liquid impacts is schematically represented in Fig. 12. The surface distortion of the ductile cobalt matrix occurred in the initial impact stage. The cumulative impacts caused severe distortion of the matrix, resulting in

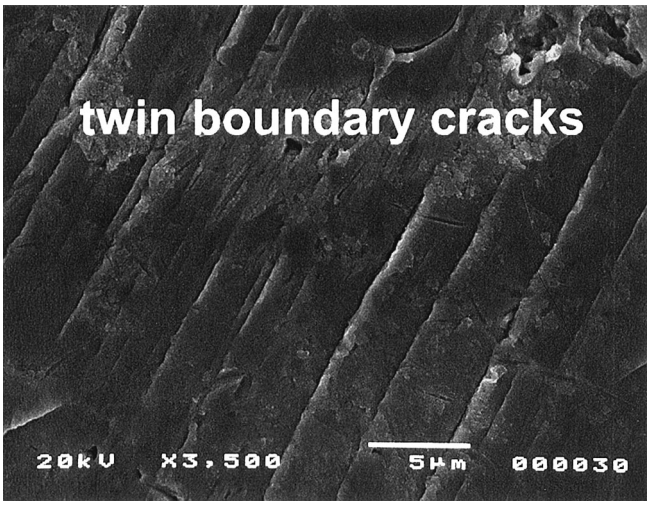


Fig. 9. Scanning electron micrographs of Stellite 6B showing the twin boundary cracks in Co matrix produced after 290 impacts at an impact velocity of 350 ± 20 m/s.

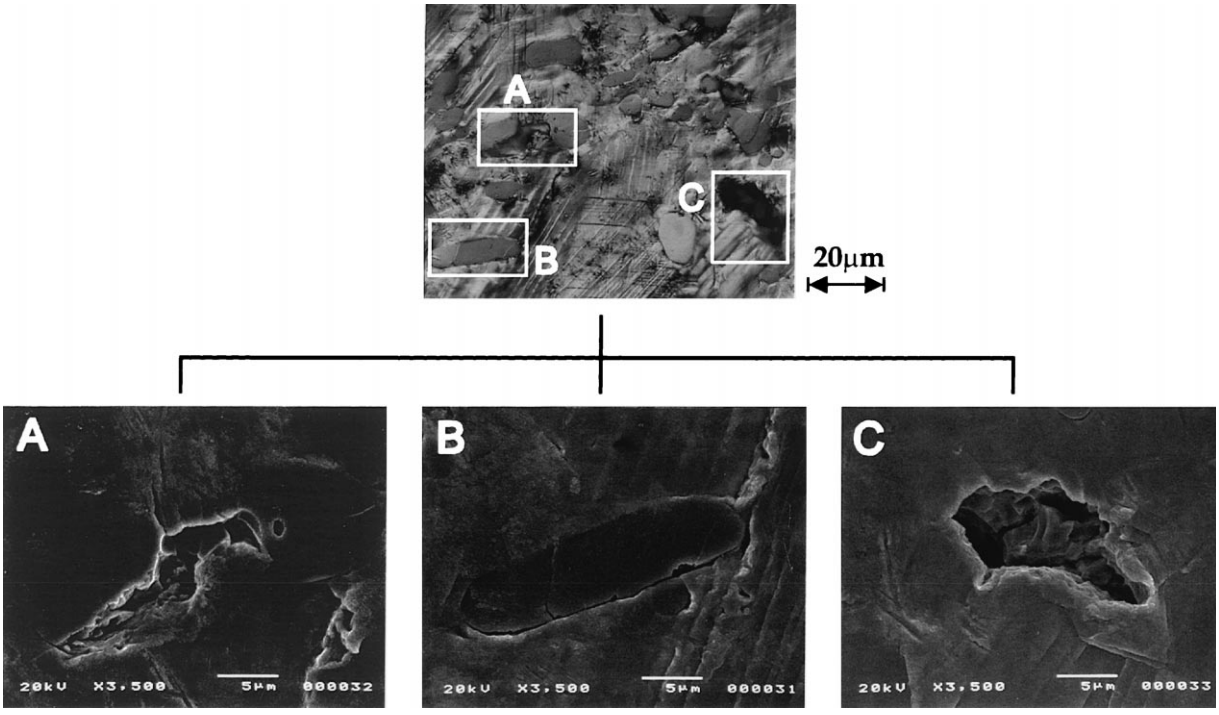


Fig. 10. Damage features of Stellite 6B produced after 290 impacts at an impact velocity of 350 ± 20 m/s.

the formation and propagation of cracks along the interface and the interior of precipitate acting as stress-concentration sites. Finally, the precipitates were fractured and removed due to combination of cracks.

It is clear that the superior erosion resistance of Stellite 6B results from the cobalt matrix whose deformation appeared as mechanical twins. Preece et al. [18] reported that since the twins had an effect of dividing the original grains into smaller segments (0.1–1.0 μm size), they confined the movement of dislocations and thereby the surface distortion. Other studies showed a trend of increasing erosion resistance with decreasing grain size

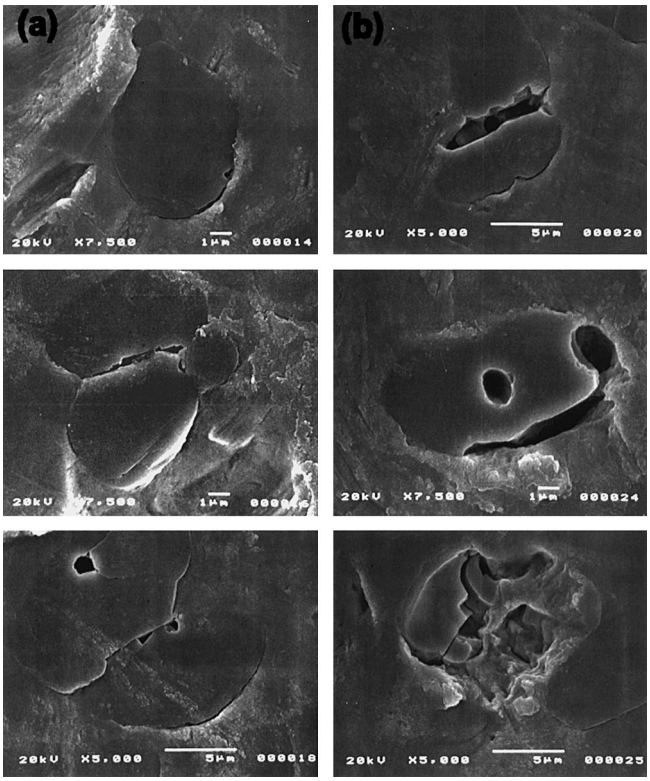


Fig. 11. Scanning electron micrographs showing: (a) the precipitate boundary cracks and (b) the fractured precipitates of Stellite 6B produced after 290 impacts at an impact velocity of 350 ± 20 m/s.

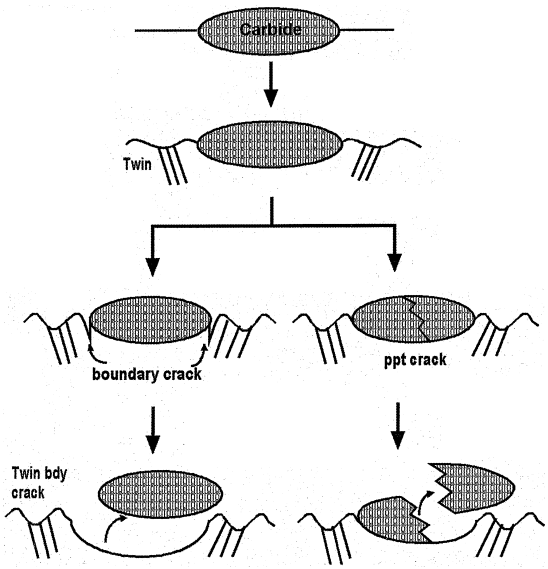


Fig. 12. Liquid impact erosion mechanism of Stellite No. 6B.

[13,16,19,20]. The twins are produced by the passage of partial dislocations which had a Burgers vector equal to a fraction of the lattice vector, giving twinned regions and untwinned regions of different orientations. Therefore, the increase in density of twins with number of impacts would play the role of fragmentation of the grains in the cobalt matrix into a submicrometer level. This would decrease the mean free path of dislocations to limit surface distortion severely and give a much higher erosion resistance.

## 4. Conclusions

1. As the impact number increased, 12Cr steel underwent a transition from ductile deformation represented by continuous surface undulations to brittle deformation by liquid impact induced work hardening.

2. In Stellite 6B, the deformation of the cobalt matrix appeared mostly as the mechanical twins and the material removal was more dominant in the hard carbide precipitates than in the ductile cobalt matrix.

3. The surface distortion of the ductile cobalt matrix occurred in the initial impact stage, whereas the deformation of the hard carbide precipitates was smaller. The cumulative impacts resulted in the formation and propagation of cracks along the interface and interior of the precipitates, followed by the selective erosion of the carbide precipitates.

## References

[1] D.W.C. Baker, D.E. Elliott, D.G. Jones, D. Pearson, Proceedings of the Second International Conference on Rain Erosion, 1967, p. 449.
[2] W. Herbert, Proceedings of the Second International Conference on Rain Erosion, 1967, p. 359.
[3] H. Rieger, Proceedings of the Third International Conference on Rain Erosion, 1970, p. 147.
[4] A. Behrendt, Proceedings of the Fourth International Conference on Rain Erosion, 1974, p. 425.
[5] R. Araki, M. Kisimoto, K. Yoshida, JSME Int. J. 34 (1991) 397.
[6] J.V. Hackworth, Proceedings of the Fifth International Conference on Erosion by Solid and Liquid Impact, Cambridge, England, September 1979, p. 10.
[7] R.I. Jaffee, Titanium steam turbine blading, Workshop Proceedings, Palo Alto, CA, 9–10 November 1988, p. 371.
[8] M. Orna, Zd. Ruml, Proceedings of the Fifth International Conference on Erosion by Solid and Liquid Impact, Cambridge, England, September 1979, p. 23.
[9] W.W. Kim, J.S. Kim, J.H. Suh, Y.S. Lim, S.S. Kim, Korean patent pending, multi impact erosion tester by water jet, 10 July 1996.
[10] G.C. Gould, Characterization and determination of erosion resistance, Symposium presented at the 72nd annual meeting, ASTM, Atlantic City, NJ, 22–27 June 1969, p. 182.
[11] F.J. Heymann, Toward Quantitative Prediction of Liquid Impact Erosion, STP 474, ASTM, 1970, p. 212.
[12] K.C. Antony, W.L. Silence, Proceedings of the Fifth international conference on erosion by liquid impact, Cambridge, England, 3–6 September 1979, p. 67.
[13] A.H. Graham, J.L. Youngblood, Metall. Trans. 1 (1970) 423.
[14] L. Remy, A. Pineau, Mater. Sci. Eng. 26 (1976) 123.
[15] D.A. Woodford, Metall. Trans. 3 (1972) 1137.
[16] S. Vaidya, S. Mahajan, C. M Preece, Metall. Trans. A 11A (1980) 1139.
[17] C.J. Heathcock, A. Ball, Wear 74 (1981) 11.
[18] C.M. Preece, S. Vaidya, S. Dakshinamoorthy, in: W.F. Adler (Ed.), Erosion: Prevention and useful applications, ASTM, 1979, p. 409.
[19] J.M. Mousson, Trans ASME 59 (1937) 399.
[20] M.J. Robinson, F.G. Hammit, Trans ASME Ser. D 89 (1967) 161.